# Nondipole electron momentum offset as a probe of correlated three-electron ionization in strongly driven atoms

G. P. Katsoulis, M. B. Peters, and A. Emmanouilidou
*Department of Physics and Astronomy, University College London, Gower Street, London WC1E 6BT, United Kingdom*

(Received 25 February 2023; revised 6 September 2023; accepted 5 October 2023; published 23 October 2023)

We employ a recently developed three-dimensional semiclassical model to identify nondipole effects in triple ionization of Ne driven by infrared laser pulses at intensities where electron-electron correlation prevails. This model fully accounts for the Coulomb interaction of each electron with the core and avoids artificial autoionization by employing effective Coulomb potentials to describe the interaction between bound electrons. Using the effective Coulomb potential for bound-bound electrons (ECBB) model, we identify a prominent signature of nondipole effects. Namely, the component along the direction of light propagation of the average sum of the final electron momenta is large and positive. That is, we identify a positive momentum offset, absent in the dipole approximation. We find that this positive momentum offset stems mostly from the momentum change due to the magnetic field. To better understand this momentum change, we also develop a simple model for the motion of an electron inside an electromagnetic field. This simple model accounts for the effect of the Coulomb forces only as a sharp change in the momentum of the electron during recollision. We show that the momentum change due to the magnetic field is related to the sharp change in momentum during recollision for the recolliding electron as well as to the time of recollision for both the recolliding and bound electrons. Hence, we demonstrate that the final electron momentum offset probes the strength of a recollision and hence the degree of correlation in multielectron ionization.

DOI: 10.1103/PhysRevA.108.043111

## I. INTRODUCTION

Nonsequential multielectron ionization (NSMI) in atoms driven by intense and infrared laser pulses is a fundamental process underlain by electron-electron correlation [1]. The theoretical study of multielectron ionization of strongly driven systems constitutes a big computational challenge. Accounting for the spatial dependence of the vector potential $\mathbf{A}(\mathbf{r},t)$ and, consequently, for the magnetic field, $\mathbf{B}(\mathbf{r},t) = \boldsymbol{\nabla}\times\mathbf{A}(\mathbf{r},t)$, adds to the computational difficulty. Hence, most theoretical studies are formulated in the dipole approximation. However, to fully explore ionization phenomena and identify nondipole effects in driven atoms and molecules one needs to account for the Lorentz force $\mathbf{F_B} = q\mathbf{v}\times\mathbf{B}$ exerted on particles of charge $q$ moving with velocity $\mathbf{v}$. Magnetic-field effects have been identified in a wide range of processes, for example, in stabilization [2], in high-harmonic generation [3–5], and in multielectron ionization probabilities of Ne [6], with observable effects found only for intensities two orders of magnitude larger than the ones considered in the current work. For the largest intensity we consider here, we find that the amplitude $\beta_0 \approx U_p/(2\omega c)$ of the electron motion due to $\mathbf{F_B}$ is roughly 0.2 a.u., where $U_p$ is the ponderomotive energy. This is much smaller than $\beta_0 \approx 1$ a.u., where, according to Refs. [7,8], magnetic-field effects are expected to arise. Over the last few years, there has been intense interest in nondipole effects [9–21]. Advanced studies [13,14] have predicted nondipole effects in correlated two-electron ionization, which have been verified experimentally for driven Ar [16]. Nondipole effects in nonsequential double ionization were also studied in a recent experiment on strongly driven Xe [18]. We previously reported *nondipole gated double ionization*, a prominent mechanism of nondipole effects in nonsequential double ionization of strongly driven atoms [13,14]. The magnetic field together with recollision acts as a gate that allows double ionization to occur only for a subset of the initial momenta of the recolliding electron along the direction of light propagation. Namely, the recolliding electron has an average initial momentum that is negative along the direction of light propagation ($y$ axis), while it is zero in the dipole approximation. The electric field is linearly polarized along the $z$ axis. This negative initial momentum compensates for the positive momentum shift induced by the Lorentz force, allowing the recolliding electron to return to the core. As a result, the recolliding electron just before recollision arrives from the $-y$ axis with positive momentum. For the case of strongly driven He at high intensities, we showed that the recollisions involved are glancing ones. As a result, the recolliding electron just before recollision is accelerated by the Coulomb attraction from the core, resulting in the $y$ component of the average sum of the final electron momenta being large and positive [13,14]. For triple ionization of Ne, for intensities where strong and not glancing recollisions prevail, we find that nondipole gated ionization is still present; that is, the recolliding electron has a negative average initial momentum. We demonstrate that the strong recollisions involved for driven Ne result in a different physical mech-

anism compared to that for driven He, still giving rise to a large positive $y$ component of the average sum of the final electron momenta. For driven Ne, using the effective Coulomb potential for bound-bound electrons (ECBB) model, we identify the change in momentum due to the magnetic field as the main source of the positive momentum offset along the $y$ axis. To better understand this momentum change, we also develop a simple model to describe the motion of an electron inside an electromagnetic field. In this simple model, we take into account the effect of the Coulomb forces via a sharp change in the momentum of each electron during recollision. Using this model, we show that for the recolliding electron the value of the positive momentum offset is analogous to the momentum change along the $z$ axis during recollision. That is, a strong recollision results in a large positive offset. Also, for both a bound electron and a recolliding electron, we find that the value of the momentum offset depends on the time of recollision. Namely, a strong recollision that takes place around a zero of the electric field results in a large positive momentum offset. Hence, in this work we demonstrate that in multielectron ionization the positive momentum offset probes the strength of the recollision involved and hence the degree of correlated electron-electron dynamics. We do so by finding a larger positive momentum offset for triple compared to double ionization and for the direct compared to the delayed recollision pathway of driven Ne. Indeed, we show that triple ionization is more correlated than double ionization and that electron-electron correlation is stronger in the direct than in the delayed pathway.

## II. METHOD

In this work, we identify nondipole effects in triple and double ionization of Ne. We use a three-dimensional (3D) semiclassical model that employs effective Coulomb potentials to describe the ECBB [22,23]. This model is developed in the nondipole framework. Moreover, this model addresses the main challenge that classical and semiclassical models of NSMI face, i.e., unphysical autoionization. Due to the singularity in the Coulomb potential, one of the bound electrons can undergo a close encounter with the core and acquire very negative energy. This leads to the escape of another bound electron via the Coulomb interaction between bound electrons. One way to avoid this is by softening the Coulomb potential; see Refs. [24–26] for nonsequential triple ionization. Alternatively, Heisenberg potentials (effective softening) [27] are added that mimic the Heisenberg uncertainty principle and prevent each electron from a close encounter with the core [28,29]. However, softening the Coulomb potential fails to accurately describe electron scattering from the core [30,31]. This renders the softened potentials quite inaccurate for high-energy recolliding electrons. In contrast, in the ECBB model, we treat exactly the Coulomb singularity in the interaction of an electron with the core as well as the interaction between a quasifree electron and a bound electron. Here, quasifree refers to a recolliding electron or an electron escaping to the continuum. To address the autoionization problem, since we treat the electron-core interaction accurately, we use an effective Coulomb potential to describe the interaction between two bound electrons. We have already shown that accurately treating the electron-core interaction is of paramount importance for obtaining accurate ionization spectra [23]. Indeed, using the ECBB model, we investigated three-electron ionization in Ar [22] and Ne [23] driven by infrared pulses. For triple ionization, we showed that the probability distribution of the sum of the final electron momenta along the $z$ axis is in very good agreement with experimental results, especially for Ne [23]. In this work, the direction of the linearly polarized electric field is along the $z$ axis. In the ECBB model, we determine on the fly whether an electron is quasifree or bound using the following simple criteria. A quasifree electron can transition to bound following a recollision. Specifically, once the quasifree electron has its closest encounter with the core, this electron transitions to bound if its position along the $z$ axis is influenced more by the core than the electric field. Also, a bound electron transitions to quasifree due to the transfer of energy during a recollision or from the laser field. In the former case, this transition occurs if the potential energy this bound electron experiences from the core is constantly decreasing. In the latter case, if the energy of the bound electron becomes positive and remains positive, it transitions to quasifree. The criteria are discussed in detail and illustrated in Refs. [22,23]. In our model, one electron tunnel ionizes through the field-lowered Coulomb barrier at time $t_0$. The tunneling occurs with a nonrelativistic quantum-mechanical tunneling rate described by the instantaneous Ammosov-Delone-Krainov (ADK) formula [32,33], adjusted accordingly to account for the depletion of the initial ground state [23]. We find $t_0$ in the time interval $[-2\tau, 2\tau]$ where the electric field is nonzero, using importance sampling [34]; $\tau$ is the full width at half maximum of the pulse duration in intensity. The exit point of the recolliding electron along the direction of the electric field is obtained analytically using parabolic coordinates [35]. The electron momentum along the electric field is set equal to zero, while the transverse one is given by a Gaussian distribution. This distribution represents the Gaussian-shaped filter with an intensity-dependent width arising from standard tunneling theory [33,36,37]. A nonrelativistic ADK rate results in this Gaussian distribution being centered around zero. In Refs. [38,39] nondipole effects were accounted for, and the most probable transverse velocities were obtained due to tunneling. However, these most probable transverse velocities, for the intensities considered in this work, are significantly smaller than the values of the average momentum along the propagation direction of the laser field obtained during time propagation; the latter average momenta are presented in what follows. For the initially bound electrons, we employ a microcanonical distribution [22], while the core is initially at rest at the origin. We use a vector potential of the form

$$\mathbf{A}(y,t) = -\frac{E_0}{\omega}\exp\left[-2\ln 2\left(\frac{ct-y}{c\tau}\right)^2\right]\sin(\omega t - ky)\hat{\mathbf{z}}, \tag{1}$$

where $k = \omega/c$ is the wave number of the laser field. The direction of the vector potential and the electric field, $\mathbf{E}(y,t) = -\frac{\partial \mathbf{A}(y,t)}{\partial t}$, is along the $z$ axis, while the direction of light propagation is along the $y$ axis. The magnetic field, $\mathbf{B}(y,t) = \boldsymbol{\nabla} \times \mathbf{A}(y,t)$, points along the $x$ axis. The pulse duration is $\tau = 25$ fs,

while the wavelength is 800 nm. We consider intensities of 1.0, 1.3, and 1.6 PW/cm$^2$. The highest intensity considered is chosen such that the probability for a second electron to tunnel ionize in Ne solely due to the laser field is very small [23]. Hence, here, electron-electron correlation prevails in triple and double ionizations. In what follows, triple ionization (TI) refers to nonsequential triple ionization (NSTI), and double ionization (DI) refers to nonsequential double ionization. The Hamiltonian of the four-body system is given by

$$H = \sum_{i=1}^{4} \frac{[\tilde{\mathbf{p}}_i - Q_i \mathbf{A}(y,t)]^2}{2m_i} + \sum_{i=2}^{4} \frac{Q_i Q_1}{|\mathbf{r}_1 - \mathbf{r}_i|} + \sum_{i=2}^{3} \sum_{j=i+1}^{4} [1 - c_{i,j}(t)] \frac{Q_i Q_j}{|\mathbf{r}_i - \mathbf{r}_j|} + \sum_{i=2}^{3} \sum_{j=i+1}^{4} c_{i,j}(t) \times [V_{\text{eff}}(\zeta_j(t), |\mathbf{r}_1 - \mathbf{r}_i|) + V_{\text{eff}}(\zeta_i(t), |\mathbf{r}_1 - \mathbf{r}_j|)], \quad (2)$$

where $Q_i$ is the charge, $m_i$ is the mass, $\mathbf{r}_i$ is the position vector, and $\tilde{\mathbf{p}}_i$ is the canonical momentum vector of particle $i$. The mechanical momentum $\mathbf{p}_i$ is given by

$$\mathbf{p}_i = \tilde{\mathbf{p}}_i - Q_i \mathbf{A}(y,t). \quad (3)$$

In the ECBB model, all electrons and the core are allowed to move [22,23]. However, at least to our knowledge, it is not currently clear how the $I_p/c$ momentum due to nondipole effects during tunneling, i.e., due to the dynamics that takes place under the field-lowered Coulomb barrier, is shared between the core and the tunneling electron as a function of laser intensity [11,39]. Hence, we consider the mass of the core to be infinite and effectively fix the core in the computations that follow. The effective Coulomb potential that an electron $i$ experiences at a distance $|\mathbf{r}_1 - \mathbf{r}_i|$ from the core (particle 1) due to the charge distribution of electron $j$ is derived as follows [22,40]. We approximate the wave function of a bound electron $j$ with a $1s$ hydrogenic wave function:

$$\psi(\zeta_j, |\mathbf{r}_1 - \mathbf{r}_j|) = \left(\frac{\zeta_j^3}{\pi}\right)^{1/2} e^{-\zeta_j |\mathbf{r}_1 - \mathbf{r}_j|}, \quad (4)$$

with $\zeta_j$ being the effective charge of particle $j$ [22,40]. Hence, using Gauss's law [22,40], we find that the potential produced due to the charge distribution $-|\psi(\zeta_j, |\mathbf{r}_1 - \mathbf{r}_j|)|^2$ is given by

$$V_{\text{eff}}(\zeta_j, |\mathbf{r}_1 - \mathbf{r}_i|) = \frac{1 - (1 + \zeta_j |\mathbf{r}_1 - \mathbf{r}_i|) e^{-2\zeta_j |\mathbf{r}_1 - \mathbf{r}_i|}}{|\mathbf{r}_1 - \mathbf{r}_i|}. \quad (5)$$

When electron $i$ approaches the core, i.e., $|\mathbf{r}_1 - \mathbf{r}_i| \to 0$, the effective potential is equal to $\zeta_j$. This ensures that the energy transfer between bound electrons is finite and therefore autoionization is prevented. The functions $c_{i,j}(t)$ determine whether at time $t$, during propagation, the full Coulomb potential or the effective $V_{\text{eff}}(\zeta_i, |\mathbf{r}_1 - \mathbf{r}_j|)$ and $V_{\text{eff}}(\zeta_j, |\mathbf{r}_1 - \mathbf{r}_i|)$ potentials describe the interaction between a pair of electrons $i$ and $j$ [22]. The effective potentials are activated on the fly only when both electrons are bound. During time propagation, to accurately account for the Coulomb singularity, we transform the position and momenta using the global regularization scheme [22,41], first introduced for the gravitational $N$-body problem [41]. We propagate in time the transformed position and momenta of all particles using the classical ECBB Hamiltonian (see [22]). To propagate, we use a leapfrog technique that allows us to solve Hamilton's equations when the derivative of the position and the momentum depends on the quantities themselves [42–44]. This technique is employed jointly with the Bulirsch-Stoer method [45,46]. We stop the propagation at time $t_f$, when the energy of each particle converges. We label the trajectory as triply or doubly ionized if three or two electrons have positive energy and compute the triple-ionization and double-ionization probabilities of all events. After we label an event as triply or doubly ionized, we identify the main pathways of energy transfer via the recollision; that is, we characterize an event as direct or delayed. We explained in detail how to identify the pathways of triple and double ionization in Refs. [22,23]. In this work we employ atomic units, unless otherwise stated.

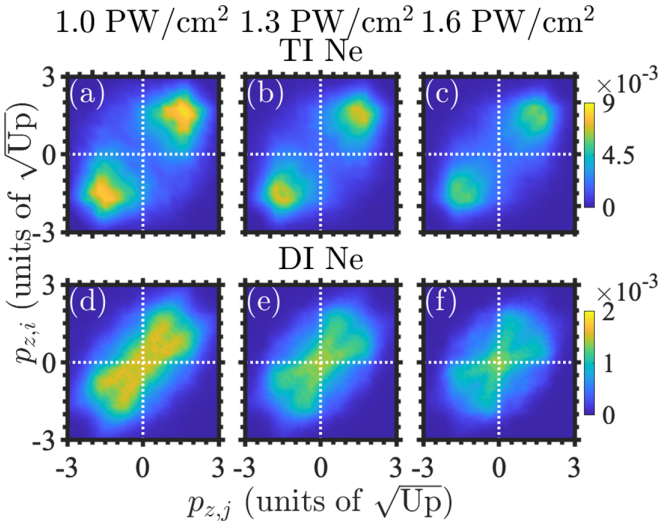


FIG. 1. For Ne, symmetrized correlated momenta $p_z$ of all three pairs of escaping electrons for triple ionization (top row) and the one pair of escaping electrons for double ionization (bottom row). Each plot is normalized to 1.

## III. RESULTS

### A. Correlated electron momenta in TI and DI

In Fig. 1, for TI and DI of driven Ne, we plot the symmetrized correlated electron momenta along the direction of the electric field $p_z$ for all pairs of escaping electrons. That is, we plot the correlated momenta for each pair of electrons, regardless of the momentum of the third electron, and then superimpose the correlated momenta of all three pairs. We find the ratio of triple to double ionization to be equal to 186, 106, and 81 for 1.0, 1.3, and 1.6 PW/cm$^2$ [23]. We find that the electron-electron dynamics is more correlated in triple ionization compared to double ionization. Specifically, for TI, at all three intensities, we find (not shown) that recollisions occur around a zero of the electric field and hence at an extremum of the vector potential. This results in large final electron momenta in TI since $p_z$ is roughly equal to minus the vector potential at the time of recollision. Indeed, this is seen in Figs. 1(a)–1(c), where we have a large concentration of electrons with large momenta in the first and third

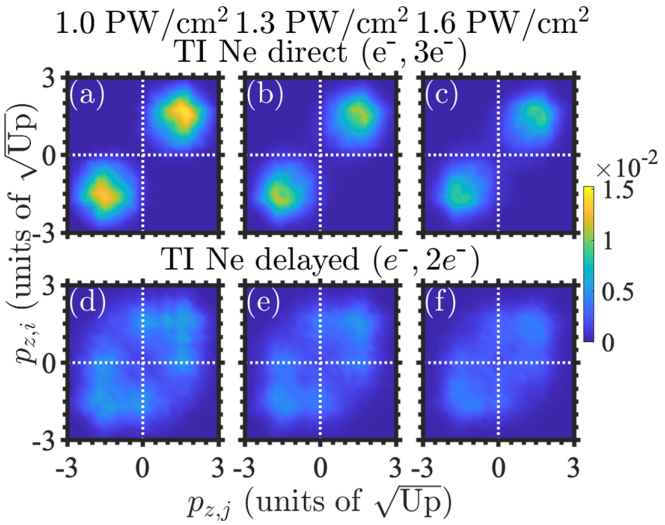


FIG. 2. For triple ionization of Ne, symmetrized correlated momenta $p_z$ for the direct $(e^-, 3e^-)$ pathway (top row) and for the delayed $(e^-, 2e^-)$ pathway (bottom row). Each plot is normalized to 1.

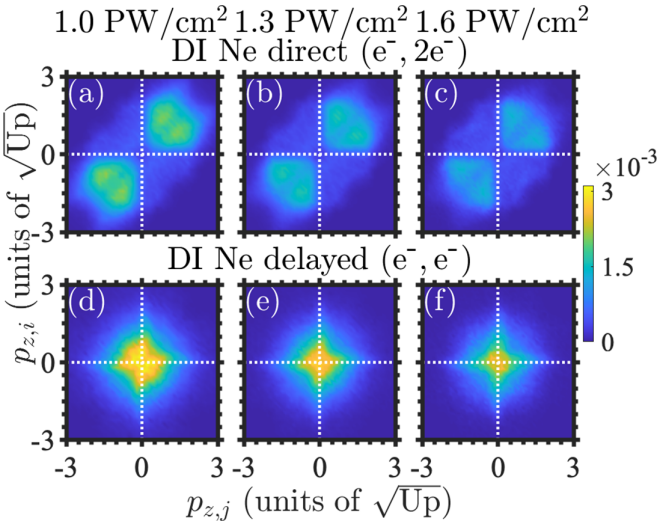


FIG. 3. For double ionization of Ne, symmetrized correlated momenta for the direct $(e^-, 2e^-)$ pathway (top row) and for the delayed $(e^-, e^-)$ pathway (bottom row). Each plot is normalized to 1.

quadrants. Comparing Figs. 1(a)–1(c) for TI with Figs. 1(d)–1(f) for DI, we find that the electron-electron dynamics is more correlated for TI. This is particularly the case at the higher intensity, 1.6 PW/cm$^2$, where we find that for DI recollisions occur more around an extremum of the field, i.e., a zero of the vector potential. This results in smaller final electron momenta for DI. Next, for TI and DI, we show that the electron-electron dynamics is more correlated for recollision pathways where more electrons ionize soon after recollision. For TI, we find that the prevailing recollision pathways are the direct $(e^-, 3e^-)$ and delayed $(e^-, 2e^-)$ pathways. The notation $(e^-, ne^-)$ denotes $n$ electrons ionizing shortly after recollision. Also, DI proceeds mainly via the direct $(e^-, 2e^-)$ and delayed $(e^-, e^-)$ pathways. We plot the symmetrized correlated electron momenta $p_z$ for the prevailing recollision pathways for TI in Fig. 2 and for DI in Fig. 3. In Fig. 2, we clearly show that the electron-electron correlation is higher in the direct pathway [Figs. 2(a)–2(c)] compared to the delayed pathway [Figs. 2(d)–2(f)]. Indeed, in Fig. 2, for TI, for the direct pathway the majority of events are concentrated in the first and third quadrants, while for the delayed pathway the events are more spread out. For DI, Fig. 3 clearly shows that electron-electron correlation is higher in the direct pathway than in the delayed pathway at all three intensities. Indeed, for DI, events for the direct pathway are concentrated in the first and third quadrants, while for the delayed pathway events are concentrated around zero momentum. Also, we find that electron-electron correlation is higher for the direct (delayed) pathway of TI compared to the direct (delayed) pathway of DI.

### B. Positive momentum offset in TI

In Fig. 4, for TI of driven Ne, to obtain the momentum offset per pair of ionizing electrons, we compute the $y$ component (direction of light propagation) of the average sum of the final electron momenta, and we then multiply by a factor of 2/3 as follows:

$$\frac{2}{3}\left\langle \sum_{i=1}^{3} p_{y,i} \right\rangle_{\text{TI}} = \left\langle \frac{(p_{y,1}+p_{y,2})+(p_{y,1}+p_{y,3})+(p_{y,2}+p_{y,3})}{3} \right\rangle. \quad (6)$$

We denote by $p_{y,i}$ the $y$ component of the final momentum of electron $i$. The reason we compute the momentum offset per pair of electrons for TI is to directly compare it with the momentum offset for DI, in which there is only one pair of

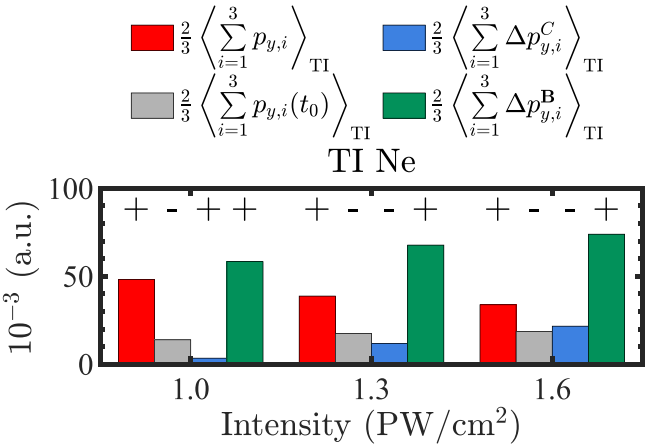


FIG. 4. For Ne, at each intensity, the height of the red bar denotes the momentum offset per pair of electrons for TI $2/3\langle\sum_{i=1}^{3} p_{y,i}\rangle$, and the contributions due to the initial momentum $2/3\langle\sum_{i=1}^{3} p_{y,i}(t_0)\rangle$ (gray bar), the magnetic field $2/3\langle\sum_{i=1}^{3} \Delta p^{\mathbf{B}}_{y,i}\rangle$ (green bar), and the Coulomb and effective potential forces $2/3\langle\sum_{i=1}^{3} \Delta p^{C}_{y,i}\rangle$ (blue bar) are also shown. The plus (+) or minus (−) sign above each bar denotes a positive or negative value, respectively, for the given contribution.

ionizing electrons. Note that the momentum offset for both TI and DI is zero in the dipole approximation. For TI, the momentum offset is denoted by the height of the red bars in Fig. 4. At all three intensities, we find that the momentum offset has a significant positive value around 0.035 a.u. We find that this is roughly four times larger than two times (to account for an electron pair) the momentum offset in single ionization. Next, we identify the reason for the positive value of the momentum offset. To do so, we write the average value of the final electron momentum $\langle p_{y,i}\rangle$ in terms of three contributions as follows:

$$\langle p_{y,i}\rangle = \langle p_{y,i}(t_0)\rangle + \langle \Delta p^{C}_{y,i}\rangle + \langle \Delta p^{\mathbf{B}}_{y,i}\rangle. \tag{7}$$

The first term, $\langle p_{y,i}(t_0)\rangle$, is the $y$ component of the average value of the initial electron momentum. The next term, $\langle \Delta p^{C}_{y,i}\rangle$, denotes the $y$ component of the average change in the momentum of electron $i$ in the time interval $[t_0, t_f]$ due to the Coulomb forces and the effective potentials, while the term $\langle \Delta p^{\mathbf{B}}_{y,i}\rangle$ denotes the corresponding momentum change due to the magnetic field. Figure 4 clearly shows that the positive momentum offset per pair of electrons for TI is due to the momentum change from the magnetic field (green bars). Figure 4 also shows that the momentum change due to the Coulomb and effective potentials forces (blue bars) is significantly less than the momentum change due to the magnetic field. Hence, in what follows, we focus on only the momentum change due to the magnetic field. The above discussion shows that for NSTI in driven Ne the mechanism responsible for the positive momentum offset along the $y$ axis is different from the nondipole gated ionization identified in strongly driven He [13]. In the latter case, the significant positive momentum offset in DI was due to the recolliding electron coming, just before recollision, mostly from the $-y$ direction with positive momentum $p_y$ and the Coulomb attraction from the core acting to increase $p_y$. However, the recollisions involved in driven He were glancing ones. For NSTI in driven Ne, we find that the recolliding electron also has a negative average initial momentum along the $y$ axis and approaches mostly from the $-y$ axis with positive $p_y$ momentum (Fig. 5). However, the recollisions in driven Ne are strong ones, resulting in the most important contribution to the $y$ component of the momentum change being due to the magnetic field and not to the Coulomb attraction from the core.

### C. Momentum change along the *y* axis

In what follows we identify the main contributions to the term $\langle \Delta p^{\mathbf{B}}_{y,i}\rangle$ in Eq. (7) for the recolliding and bound electrons. We find $\Delta p^{\mathbf{B}}_{y,i}$ using a simple model of an electron inside an electromagnetic field and account for the effect of the

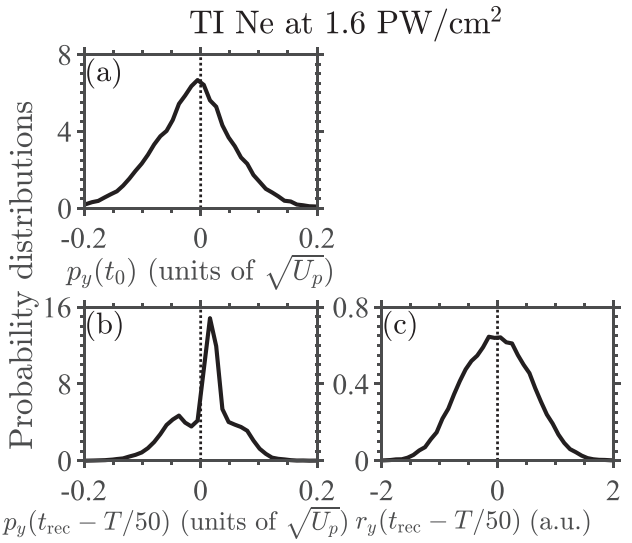


FIG. 5. Plots of the distribution of the $y$ component of the momentum of the recolliding electron (a) at the time of tunneling $t_0$ and (b) shortly before recollision at time $t_{\rm rec} - T/50$ and (c) of the $y$ component of the position of the recolliding electron shortly before recollision at time $t_{\rm rec} - T/50$ for TI of driven Ne at 1.6 PW/cm$^2$. $T$ is the period of the laser field.

Coulomb forces with a sharp change during recollision in the momentum of each electron $[\Delta p_{z,i}(t_{\rm rec})]$.

#### 1. *Momentum change along the* y *axis for a recolliding electron*

The Lorentz force acting on an electron $i$ is

$$\mathbf{F}_{\rm L} = -[\mathbf{E}(y_i, t) + \mathbf{p}_i \times \mathbf{B}(y_i, t)]. \tag{8}$$

The momentum of electron $i$ at time $t$ is then given by

$$\mathbf{p}_i(t) = \mathbf{p}_i(t_0) - \int_{t_0}^{t} [\mathbf{E}(y_i, t') + \mathbf{p}_i \times \mathbf{B}(y_i, t')]dt'. \tag{9}$$

Equation (9) does not account for the Coulomb interaction between an electron and the core as well as between electrons. In a simplified model for the recolliding electron, we account for the momentum change due to a recollision and hence due to the Coulomb forces by adding a term in (9) as follows:

$$\mathbf{p}_i(t) = \mathbf{p}_i(t_0) - \int_{t_0}^{t} [\mathbf{E}(y_i, t') + \mathbf{p}_i \times \mathbf{B}(y_i, t')]dt' + \mathrm{H}(t - t_{\rm rec})\Delta\mathbf{p}_i(t_{\rm rec}), \tag{10}$$

where $\mathrm{H}(t - t_{\rm rec})$ is the Heaviside function [47] and $\Delta\mathbf{p}_i(t_{\rm rec})$ is the momentum change due to the Coulomb forces just after and before the recollision time $t_{\rm rec}$. Then from Eq. (10) it follows that the $y$ component of the momentum change due to the magnetic field for $t > t_{\rm rec}$ takes the form

$$\Delta p^{\mathbf{B}}_{y,i}(t_0 \to t) = -\int_{t_0}^{t} p_{z,i}(t')B(y_i, t')dt'$$
$$= -\int_{t_0}^{t}\left[p_{z,i}(t_0) - \int_{t_0}^{t'} E(y_i, t'')dt'' + \int_{t_0}^{t'} p_{y,i}(t'')B(y_i, t'')dt'' + \mathrm{H}(t' - t_{\rm rec})\Delta p_{z,i}(t_{\rm rec})\right]B(y_i, t')dt'$$

$$= -\int_{t_0}^{t}\left[p_{z,i}(t_0) - \int_{t_0}^{t'} E(y_i,t'')dt'' + \int_{t_0}^{t'} p_{y,i}(t'')B(y_i,t'')dt''\right]B(y_i,t')dt' - \Delta p_{z,i}(t_{\rm rec})\int_{t_{\rm rec}}^{t} B(y_i,t')dt'$$

$$= \Delta p_{y,i}^{\mathbf{B},1}(t_0 \to t) - \Delta p_{z,i}(t_{\rm rec})\int_{t_{\rm rec}}^{t} B(y_i,t')dt' = \Delta p_{y,i}^{\mathbf{B},1}(t_0 \to t) + \Delta p_{y,i}^{\mathbf{B},2}(t_{\rm rec} \to t). \quad (11)$$

The term $\Delta p_{y,i}^{\mathbf{B},1}(t_0 \to t)$ simplifies when we take into account that in our model the initial momentum of the recolliding electron along the direction of the electric field is zero, $p_{z,i}(t_0) = 0$. Furthermore, for the purposes of this model we neglect terms of the order of $\mathbf{B}^2$ since the ratio of the magnitudes of the electric and magnetic fields is $|E(y_i,t)/B(y_i,t)| = c$. Another approximation we make for the purposes of this model is that we compute the integral of the magnetic and electric fields over time at the position $y_i = 0$. That is,

$$E(y_i,t) \approx E(0,t) \equiv E(t), \quad (12)$$

$$B(y_i,t) \approx B(0,t) \equiv B(t). \quad (13)$$

Given the above approximations, we find that

$$\Delta p_{y,i}^{\mathbf{B},1}(t_0 \to t) = \int_{t_0}^{t}\left[\int_{t_0}^{t'} E(t'')dt''\right]B(t')dt', \quad (14a)$$

$$\Delta p_{y,i}^{\mathbf{B},2}(t_{\rm rec} \to t) = -\Delta p_{z,i}(t_{\rm rec})\int_{t_{\rm rec}}^{t} B(t')dt'. \quad (14b)$$

For the recolliding electron, at all three intensities for both TI and DI, we find that the term $\Delta p_{y,i}^{\mathbf{B},2}(t_{\rm rec} \to t_f)$ contributes the most to $\Delta p_{y,i}^{\mathbf{B}}(t_0 \to t_f)$. We find that this is the case by using $\Delta p_{z,i}(t_r ec)$ from our full calculations using the ECBB model. Next, we show that $\Delta p_{y,i}^{\mathbf{B},2}(t_{\rm rec} \to t_f)$ is always positive. Indeed, we rewrite Eq. (14b) as

$$\Delta p_{y,i}^{\mathbf{B},2}(t_{\rm rec} \to t_f) = -\Delta p_{z,i}(t_{\rm rec})\int_{t_{\rm rec}}^{t_f}\frac{E(t)}{c}dt$$

$$= -\frac{1}{c}\Delta p_{z,i}(t_{\rm rec})[A(t_{\rm rec}) - A(t_f)]$$

$$= -\frac{1}{c}\Delta p_{z,i}(t_{\rm rec})A(t_{\rm rec}), \quad (15)$$

where we use $\mathbf{E}(t) = -\frac{\partial \mathbf{A}(t)}{\partial t}$ and $A(t_f \to \infty) = 0$. Moreover, for the tunneling or recolliding electron, we find that

$$p_{z,i}(t_{\rm rec}) = -\int_{t_0}^{t_{\rm rec}} E(t)dt$$

$$= -[A(t_0) - A(t_{\rm rec})]$$

$$= A(t_{\rm rec}), \quad (16)$$

where we have used $A(t_0) \approx 0$ since the electron tunnels at an initial time $t_0$ around an extremum of the electric field. Then Eq. (15) can be written as

$$\Delta p_{y,i}^{\mathbf{B},2}(t_{\rm rec} \to t_f) = -\frac{1}{c}\Delta p_{z,i}(t_{\rm rec})p_{z,i}(t_{\rm rec})$$

$$= -\frac{1}{c}[p_{z,i}(t_{\rm rec} + \Delta t) - p_{z,i}(t_{\rm rec})]p_{z,i}(t_{\rm rec}). \quad (17)$$

During a recollision, the magnitude of the momentum of the recolliding electron after the recollision is always smaller than its magnitude before the recollision. Hence, we can easily show that $\Delta p_{y,i}^{\mathbf{B},2}(t_{\rm rec} \to t_f)$ is always greater than zero.

#### 2. *Momentum change along the* y *axis for a bound electron*

Concerning a bound electron, we assume that the electron feels the electric and magnetic fields only after it is ionized, i.e., roughly at the recollision time. Hence, for the bound electron, in (10) and (11) we substitute $t_0$ by $t_{\rm rec}$. We also assume that $p_i(t_{\rm rec}) \approx 0$. Given the above assumptions, we find that

$$\Delta p_{y,i}^{\mathbf{B}}(t_{\rm rec} \to t) = \int_{t_{\rm rec}}^{t}\left[\int_{t_{\rm rec}}^{t'} E(t'')dt''\right]B(t')dt'$$

$$- \Delta p_{z,i}(t_{\rm rec})\int_{t_{\rm rec}}^{t} B(t')dt'$$

$$= \Delta p_{y,i}^{\mathbf{B},1}(t_{\rm rec} \to t) + \Delta p_{y,i}^{\mathbf{B},2}(t_{\rm rec} \to t). \quad (18)$$

For both TI and DI, at all three intensities, we find that the term $\Delta p_{y,i}^{\mathbf{B},1}(t_{\rm rec} \to t_f)$ contributes the most to $\Delta p_{y,i}^{\mathbf{B}}(t_{\rm rec} \to t_f)$ for the bound electron. Next, we show that this term is always positive as follows:

$$\Delta p_{y,i}^{\mathbf{B},1}(t_{\rm rec} \to t_f) = \int_{t_{\rm rec}}^{t_f}\left[\int_{t_{\rm rec}}^{t} E(t')dt'\right]B(t)dt$$

$$= \int_{t_{\rm rec}}^{t_f}[A(t_{\rm rec}) - A(t)]B(t)dt$$

$$= A(t_{\rm rec})\int_{t_{\rm rec}}^{t_f} B(t)dt - \int_{t_{\rm rec}}^{t_f} A(t)B(t)dt$$

$$= \frac{A(t_{\rm rec})}{c}[A(t_{\rm rec}) - A(t_f)] - \int_{t_{\rm rec}}^{t_f} A(t)\frac{E(t)}{c}dt$$

$$= \frac{1}{c}\left[A^2(t_{\rm rec}) + \frac{A^2(t_f)}{2} - \frac{A^2(t_{\rm rec})}{2}\right]$$

$$= \frac{1}{2c}A^2(t_{\rm rec}) > 0, \quad (19)$$

where we use $A(t_f \to \infty) = 0$.

### D. Comparison of the offset between DI and TI

In Fig. 6, for DI of driven Ne, we compute the $y$ component of the average sum of the final momenta of the ionizing electron pair $\langle\sum_{i=1}^{2} p_{y,i}\rangle_{\rm DI}$. This momentum offset is denoted by the height of the red bar. At intensities 1.0 and 1.3 PW/cm$^2$ we find that the momentum offset has a positive value around 0.03 a.u. This is roughly three times larger than two time (to account for the electron pair) the momentum offset in single ionization. At an intensity of 1.6 PW/cm$^2$ the value of the positive momentum offset is approximately half its value at

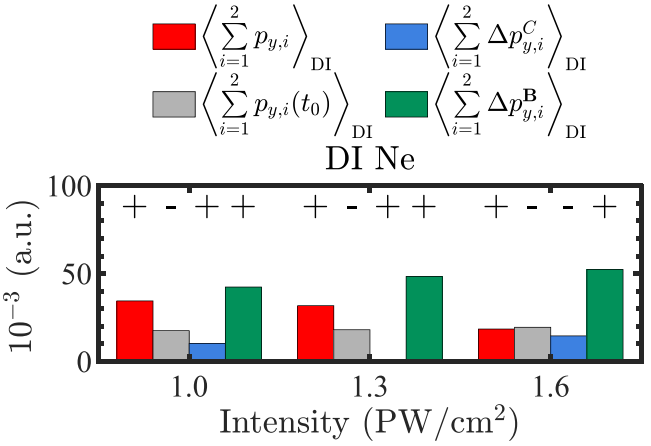


FIG. 6. For Ne, at each intensity, the height of the red bar denotes the momentum offset per pair of electrons for DI $\langle\sum_{i=1}^{2} p_{y,i}\rangle$, and the contributions due to the initial momentum $\langle\sum_{i=1}^{2} p_{y,i}(t_0)\rangle$ (gray bar), the magnetic field $\langle\sum_{i=1}^{2} \Delta p_{y,i}^{\mathbf{B}}\rangle$ (green bar), and the Coulomb and effective potential forces $\langle\sum_{i=1}^{2} \Delta p_{y,i}^{C}\rangle$ (blue bar) are also shown. The plus (+) or minus (−) sign above each bar denotes a positive or negative value, respectively, for the given contribution.

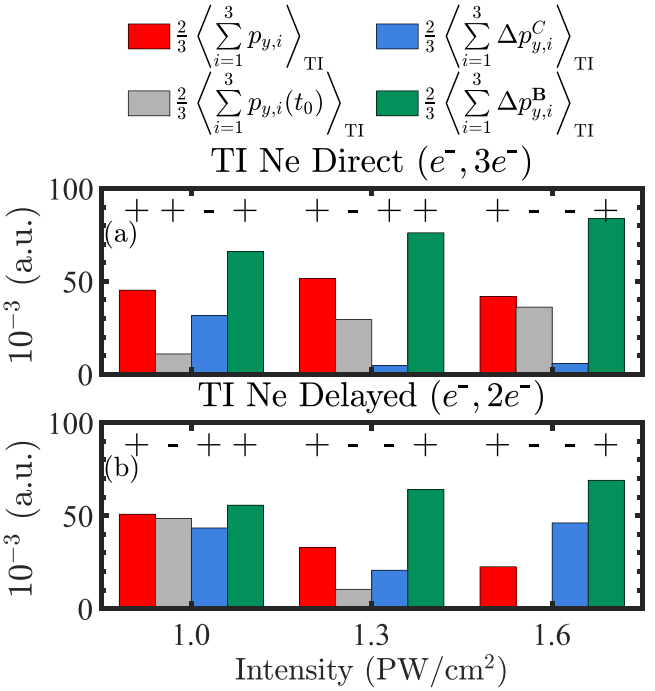


FIG. 7. For Ne, at each intensity, the height of the red bar denotes the momentum offset per pair of electrons for TI $2/3\langle\sum_{i=1}^{3} p_{y,i}\rangle$, and the contributions due to the magnetic field $2/3\langle\sum_{i=1}^{3} \Delta p_{y,i}^{\mathbf{B}}\rangle$ (green bar), due to the initial momentum $2/3\langle\sum_{i=1}^{3} p_{y,i}(t_0)\rangle$ (gray bar), and due to the Coulomb and effective potential forces $2/3\langle\sum_{i=1}^{3} \Delta p_{y,i}^{C}\rangle$ (blue bar) are also shown. The plus (+) or minus (−) sign above each bar denotes a positive or negative value, respectively, for the given contribution. (a) corresponds to the direct $(e^-, 3e^-)$ pathway, and (b) corresponds to the delayed $(e^-, 2e^-)$ pathway.

the two smaller intensities. Figure 6 clearly shows that the positive momentum offset for DI is due to the momentum change from the magnetic field (green bars), as was the case for TI. At all three intensities, we find that for triple ionization $2/3\langle\sum_{i=1}^{3} \Delta p_{y,i}^{\mathbf{B}}\rangle$ ranges roughly from 0.06 to 0.07 a.u. (green bars in Fig. 4), while for double ionization $\langle\sum_{i=1}^{2} \Delta p_{y,i}^{\mathbf{B}}\rangle$ is smaller, ranging roughly from 0.04 to 0.05 a.u. (green bars in Fig. 6).

Now, we show that the smaller positive momentum offset due to the magnetic field in double ionization compared to triple ionization is consistent with the simple model developed in Sec. III C. Indeed, recollisions are stronger in TI versus DI. This is evidenced by the higher degree of electron-electron correlation in TI compared to DI (compare the top and bottom rows in Fig. 1). A stronger recollision in TI translates to a larger change in the $z$ component of the momentum of the recolliding electron due to the Coulomb forces during recollision, i.e., to a larger value of $\Delta p_{z,i}(t_{\rm rec})$ in Eq. (15). Moreover, a stronger recollision also translates to the time of recollision being around a zero of the electric field, resulting in an extremum of $A(t_{\rm rec})$. Hence, the most important contributions to the momentum offset, the term $\Delta p_{y,i}^{\mathbf{B},2}(t_{\rm rec} \to t_f)$ for the recolliding electron [Eq. (15)] and the term $\Delta p_{y,i}^{\mathbf{B},1}(t_{\rm rec} \to t_f)$ for the bound electron [Eq. (19)], have larger values for TI compared to DI.

### E. Momentum offset for direct versus delayed pathways in TI and DI

In what follows, we compare the momentum offset in the direct pathway versus the delayed pathway in both TI and DI. In Fig. 7, for TI of driven Ne, we show the momentum offset (red bars), the contribution to this offset from the magnetic field (green bars), and the contribution from the Coulomb and effective potential forces (blue bars) for the direct [Fig. 7(a)] and delayed $(e^-, 2e^-)$ [Fig. 7(b)] pathways. For the two highest intensities we find that the momentum offset (red bars) is larger in the direct pathway than in the delayed pathway. Figure 7 clearly shows that this is mainly due to the larger positive values of the momentum change due to the magnetic field (green bars) in the direct pathway compared to the delayed pathway. That is, the term $2/3\langle\sum_{i=1}^{3} \Delta p_{y,i}^{\mathbf{B}}\rangle$ is larger in the direct pathway than in the delayed pathway. Figure 8 shows that the same holds true for DI of driven Ne for all three intensities. That is, the momentum offset, as well as the contribution to this offset from the magnetic field $\langle\sum_{i=1}^{2} \Delta p_{y,i}^{\mathbf{B}}\rangle$, is larger in the direct pathway than in the delayed pathway. Next, we explain why this is the case. During recollision, the recolliding electron gives more energy to the bound electrons in the direct pathway compared to the delayed pathway. That is, the sharp momentum change in the recolliding electron during recollision $\Delta p_{z,i}(t_{\rm rec})$ is larger in the direct pathway than in the delayed pathway. Hence, $\Delta p_{y,i}^{\mathbf{B},2}(t_{\rm rec} \to t_f)$ in Eq. (15) for the recolliding electron is larger in the direct pathway. In addition, for the bound electrons, $\Delta p_{y,i}^{\mathbf{B},1}(t_{\rm rec} \to t_f)$ in Eq. (19) is larger in the direct pathway than in the delayed pathway. The reason is that both bound electrons in the direct pathway ionize soon after the recollision time, which is around an extremum of the vector potential $A$, i.e., maximum value of $A(t_{\rm rec})$. However, in the delayed pathway, most likely, it is one of the bound electrons that ionizes with a delay from the recollision time, and hence, $A(t_{\rm rec})$ is smaller than its extremum value.

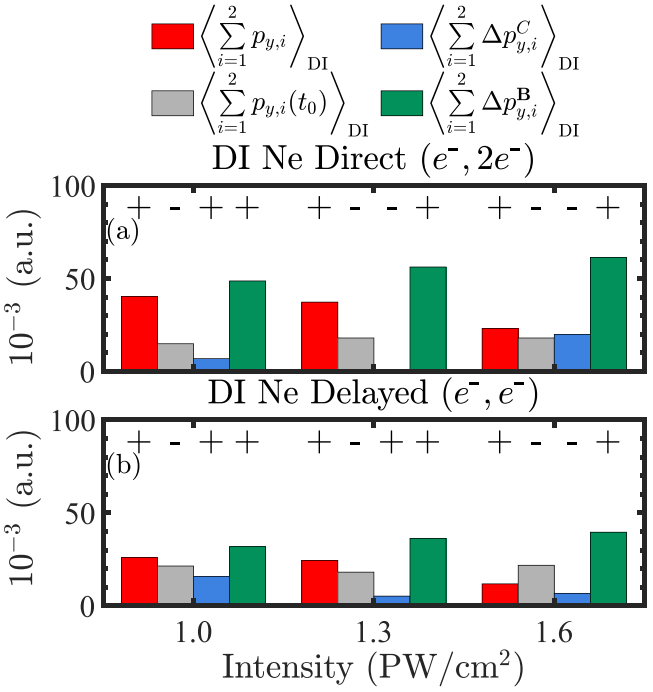


FIG. 8. For Ne, at each intensity, the height of the red bar denotes the momentum offset per pair of electrons for DI $\langle\sum_{i=1}^{2} p_{y,i}\rangle$, and the contributions due to the magnetic field $\langle\sum_{i=1}^{2} \Delta p_{y,i}^{\mathbf{B}}\rangle$ (green bar), due to the initial momentum $\langle\sum_{i=1}^{2} p_{y,i}(t_0)\rangle$ (gray bar), and due to Coulomb and effective potential forces $\langle\sum_{i=1}^{2} \Delta p_{y,i}^{C}\rangle$ (blue bar) are also shown. The plus (+) or minus (−) sign above each bar denotes a positive or negative value, respectively, for the given contribution. (a) corresponds to the direct $(e^-, 2e^-)$ pathway, and (b) corresponds to the delayed $(e^-, e^-)$ pathway.

Finally, we note that the contribution of the momentum change due to the Coulomb and effective potential forces along the $y$ axis $\frac{2}{3}\langle\sum_{i=1}^{3} \Delta p_{y,i}^{C}\rangle$ (see Fig. 4) is larger for the delayed pathway than for the direct pathway of TI. This is consistent with the electrons spending more time around the core in the weaker recollisions that take place in the delayed pathway compared to the direct pathway of TI. Moreover, we find that the contribution of the momentum change due to the Coulomb and effective potential forces along the $y$ axis is larger for the delayed pathway of TI pathway than for the delayed pathway of DI. This is consistent with the net core charge that is seen by an escaping electron in TI being equal to 3 versus 2 in DI.

## IV. CONCLUSIONS

In conclusion, we used the ECBB 3D semiclassical model to identify nondipole effects in triple and double ionizations in Ne driven by infrared pulses for intensities where recollisions, i.e., electron-electron correlation, prevail. We found a large positive average sum of the final electron momenta along the direction of light propagation. This momentum offset is zero in the absence of magnetic field. Most importantly, we showed this final electron momentum offset is a probe of the electron-electron correlation. Indeed, we found a larger momentum offset for the more correlated electron-electron ionization (i) in triple compared to double ionization of driven Ne, especially at high intensities, and (ii) in the direct versus delayed pathway of triple and double ionizations of Ne. The nondipole effects identified here in multielectron ionization observables can be accessed and hence verified by future experiments.

## ACKNOWLEDGMENTS

A.E. and G.P.K. acknowledge EPSRC Grant No. EP/W005352/1. The authors acknowledge the use of the UCL Myriad High Performance Computing Facility (Myriad@UCL), the use of the UCL Kathleen High Performance Computing Facility (Kathleen@UCL), and associated support services in the completion of this work.

[1] A. l'Huillier, L. A. Lompre, G. Mainfray, and C. Manus, Phys. Rev. A **27**, 2503 (1983).
[2] M. Y. Emelin and M. Y. Ryabikin, Phys. Rev. A **89**, 013418 (2014).
[3] C. C. Chirilă, N. J. Kylstra, R. M. Potvliege, and C. J. Joachain, Phys. Rev. A **66**, 063411 (2002).
[4] M. W. Walser, C. H. Keitel, A. Scrinzi, and T. Brabec, Phys. Rev. Lett. **85**, 5082 (2000).
[5] C. H. Keitel and P. L. Knight, Phys. Rev. A **51**, 1420 (1995).
[6] S. Palaniyappan, A. DiChiara, E. Chowdhury, A. Falkowski, G. Ongadi, E. L. Huskins, and B. C. Walker, Phys. Rev. Lett. **94**, 243003 (2005).
[7] H. R. Reiss, Phys. Rev. Lett. **101**, 043002 (2008).
[8] H. R. Reiss, J. Phys. B **47**, 204006 (2014).
[9] C. T. L. Smeenk, L. Arissian, B. Zhou, A. Mysyrowicz, D. M. Villeneuve, A. Staudte, and P. B. Corkum, Phys. Rev. Lett. **106**, 193002 (2011).
[10] A. Ludwig, J. Maurer, B. W. Mayer, C. R. Phillips, L. Gallmann, and U. Keller, Phys. Rev. Lett. **113**, 243001 (2014).
[11] S. Chelkowski, A. D. Bandrauk, and P. B. Corkum, Phys. Rev. Lett. **113**, 263005 (2014).
[12] B. Wolter, M. G. Pullen, M. Baudisch, M. Sclafani, M. Hemmer, A. Senftleben, C. D. Schröter, J. Ullrich, R. Moshammer, and J. Biegert, Phys. Rev. X **5**, 021034 (2015).
[13] A. Emmanouilidou and T. Meltzer, Phys. Rev. A **95**, 033405 (2017).
[14] A. Emmanouilidou, T. Meltzer, and P. B. Corkum, J. Phys. B **50**, 225602 (2017).
[15] B. Willenberg, J. Maurer, B. W. Mayer, and U. Keller, Nat. Commun. **10**, 5548 (2019).
[16] F. Sun, X. Chen, W. Zhang, J. Qiang, H. Li, P. Lu, X. Gong, Q. Ji, K. Lin, H. Li, J. Tong, F. Chen, C. Ruiz, J. Wu, and F. He, Phys. Rev. A **101**, 021402(R) (2020).
[17] K. Lin, S. Brennecke, H. Ni, X. Chen, A. Hartung, D. Trabert, K. Fehre, J. Rist, X.-M. Tong, J. Burgdörfer, L. P. H. Schmidt,

M. S. Schöffler, T. Jahnke, M. Kunitski, F. He, M. Lein, S. Eckart, and R. Dörner, Phys. Rev. Lett. **128**, 023201 (2022).
[18] K. Lin, X. Chen, S. Eckart, H. Jiang, A. Hartung, D. Trabert, K. Fehre, J. Rist, L. P. H. Schmidt, M. S. Schöffler, T. Jahnke, M. Kunitski, F. He, and R. Dörner, Phys. Rev. Lett. **128**, 113201 (2022).
[19] A. Hartung, S. Eckart, S. Brennecke, J. Rist, D. Trabert, K. Fehre, M. Richter, H. Sann, S. Zeller, K. Henrichs, G. Kastirke, J. Hoehl, A. Kalinin, M. S. Schöffler, T. Jahnke, L. P. H. Schmidt, M. Lein, M. Kunitski, and R. Dörner, Nat. Phys. **15**, 1222 (2019).
[20] S. Chelkowski, A. D. Bandrauk, and P. B. Corkum, Phys. Rev. A **92**, 051401(R) (2015).
[21] S. Brennecke and M. Lein, J. Phys. B **51**, 094005 (2018).
[22] M. B. Peters, G. P. Katsoulis, and A. Emmanouilidou, Phys. Rev. A **105**, 043102 (2022).
[23] A. Emmanouilidou, M. B. Peters, and G. P. Katsoulis, Phys. Rev. A **107**, L041101 (2023).
[24] P. J. Ho and J. H. Eberly, Phys. Rev. Lett. **97**, 083001 (2006).
[25] Y. Zhou, Q. Liao, and P. Lu, Opt. Express **18**, 16025 (2010).
[26] Q. Tang, C. Huang, Y. Zhou, and P. Lu, Opt. Express **21**, 21433 (2013).
[27] C. L. Kirschbaum and L. Wilets, Phys. Rev. A **21**, 834 (1980).
[28] H. Jiang and F. He, Phys. Rev. A **104**, 023113 (2021).
[29] H. Jiang, D. Efimov, F. He, and J. S. Prauzner-Bechcicki, Phys. Rev. A **105**, 053119 (2022).
[30] R. R. Pandit, Y. Sentoku, V. R. Becker, K. Barrington, J. Thurston, J. Cheatham, L. Ramunno, and E. Ackad, Phys. Plasmas **24**, 073303 (2017).
[31] R. R. Pandit, V. R. Becker, K. Barrington, J. Thurston, L. Ramunno, and E. Ackad, Phys. Plasmas **25**, 043302 (2018).
[32] L. D. Landau and E. M. Lifshitz, *Quantum Mechanics: Non-relativistic Theory*, 2nd ed. (Pergamon, Oxford, 1965).
[33] N. B. Delone and V. P. Krainov, J. Opt. Soc. Am. B **8**, 1207 (1991).
[34] R. Y. Rubinstein and D. P. Froese, *Simulation and the Monte Carlo Method*, 3rd ed. (Wiley, Hoboken, NJ, 2016).
[35] B. HuP, J. Liu, and S.-G. Chen, Phys. Lett. A **236**, 533 (1997).
[36] N. B. Delone and V. P. Krainov, Phys. Usp. **41**, 469 (1998).
[37] L. Fechner, N. Camus, J. Ullrich, T. Pfeifer, and R. Moshammer, Phys. Rev. Lett. **112**, 213001 (2014).
[38] E. Yakaboylu, M. Klaiber, H. Bauke, K. Z. Hatsagortsyan, and C. H. Keitel, Phys. Rev. A **88**, 063421 (2013).
[39] P.-L. He, M. Klaiber, K. Z. Hatsagortsyan, and C. H. Keitel, Phys. Rev. A **105**, L031102 (2022).
[40] V. J. Montemayor and G. Schiwietz, Phys. Rev. A **40**, 6223 (1989).
[41] D. C. Heggie, Celestial Mech. **10**, 217 (1974).
[42] P. Pihajoki, Celestial Mech. Dyn. Astron. **121**, 211 (2015).
[43] L. Liu, X. Wu, G. Huang, and F. Liu, Mon. Not. R. Astron. Soc. **459**, 1968 (2016).
[44] G. P. Katsoulis, M. B. Peters, A. Staudte, R. Bhardwaj, and A. Emmanouilidou, Phys. Rev. A **103**, 033115 (2021).
[45] W. H. Press, S. A. Teukolsky, W. T. Vetterling, and B. P. Flannery, *Numerical Recipes: The Art of Scientific Computing*, 3rd ed. (Cambridge University Press, Cambridge, 2007).
[46] R. Bulirsch and J. Stoer, Numer. Math. **8**, 1 (1966).
[47] M. Abramowitz and I. Stegun, *Handbook of Mathematical Functions: With Formulas, Graphs, and Mathematical Tables*, Applied Mathematics Series (Dover Publications, Inc., New York, 1965).